Mitigating harbor storms by enhancing nonlinear wave interactions

Paul Chleboun
Complexity DTC, Zeeman Building, University of Warwick, Coventry CV4 7AL, UK
(Dated: April 16, 2009)

We analyse results for surface gravity water wave turbulence in a finite flume with one or two excited wave modes. We discuss the results in relation to established wave theory and recent predictions for wave turbulence in finite regions. It is proposed that an initial maximum in the surface elevation can be explained in terms of a reduction in exact and quasi resonances due to k-space discreteness imposed by the finite size. The implications to Harbour design are discussed and it is suggested that exciting Eigen modes of the flume that almost satisfy resonance conditions and are predicted to interact with the driving modes to cause transfer of energy over scales could reduce the effect of the initial maximum.

I. INTRODUCTION

Understanding the evolution of surface gravity waves is of great importance for many applications, including navigation and industrial activities at sea. For example waves with wavelengths of tens of meters can pose serious dangers to ships docked in oceanic harbours. Gravity waves in such systems are forced by wind and waves coming from the ocean. Energy dissipation primarily occurs at short wavelengths via wave breaking and white-capping. It is therefore of interest how energy is transferred from the long to short wave lengths. This article focuses on investigating possible effects of the finite size on evolution of surface gravity waves with the intent that enhancing the transfer of energy to smaller scales could be useful in future harbour design.

There exists a well developed theory for wave fields on an unbounded surface where the wave field is assumed to be random (such as surface gravity waves on the ocean), see for example [1]. The theory describing these fields is known as Wave Turbulence (WT). In 1962 Hasselmann derived a kinetic equation for the transfer of energy in surface gravity waves [2]. Later Zakharov and Filonenko found an exact solution to the wave kinetic equation in the form of a Kolmogorov type energy cascade describing the transfer of energy from low frequencies to high frequency where energy is dispersed by wave breaking. The solution takes the form of a power law power spectrum [3].

For application to a finite region such as harbours fundamental assumptions made in WT are never met (this is also the case for numerical simulations). Recently the effects of such a restriction have been studied with regards to the predictions made by WT, with focus on the implications to numerical simulations [4, 7–9]. In particular recent studies have predicted significant differences in the form of the energy cascade compared to WT due to the k-space discreteness imposed by a restriction to a finite region [7]. However due to the restrictions of current numerical simulations (such as short inertial range) it is difficult to confirm some of these predictions. Some of the implications of the theory described in [7] have been investigate in experiments in a laboratory flume which demonstrated that the conditions require for WT to be applicable were not met [10].

In this paper we examine results from an experiment in a laboratory flume with the same setup as in [10]. Our focus is on the energy cascade from low frequencies (at which waves are excited) to higher frequencies and compare results to WT and recent predictions. We find that the surface elevation has an initial maximum (a scenario that could be dangerous in oceanic harbours) and propose that it can be at least partial explained by finite size effects. We then discuss the possibility of reducing such an effect by exciting other ('well chosen') wave modes in the flume.

II. BACKGROUND THEORY

A. Introduction

We briefly overview some relevant theory of gravity driven waves on the surface of an incompressible irrotational fluid. Let z be the vertical coordinate directed upwards with its origin $z = 0$ on the undisturbed surface. The equation of the free surface is given by $z = \eta(\mathbf{x}, t)$, where $\mathbf{x} = (x, y)$. The fluid is bounded below by a flat surface at $z = -h$ and is under the action of a gravity field $-g\hat{\mathbf{z}}$. Since the fluid flow is assumed to be irrotational the velocity $\mathbf{u}$ can be expressed as the gradient of a potential ϕ. The in-compressibility condition, $\nabla \cdot \mathbf{u} = 0$, therefore imposes the Laplace equation on the potential ϕ,

$$\Delta\phi = 0. \tag{1}$$

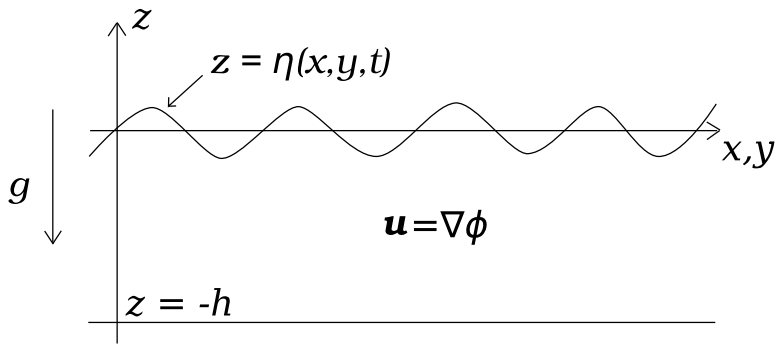

FIG. 1: Gravity waves on the free surface of an irrotational fluid bounded below by a flat surface at $z = -h$.

We further introduce notation for the velocity potential evaluated at the fluid surface,

$$\psi(\mathbf{x}, t) = \phi(\mathbf{x}, \eta(\mathbf{x}, t), t). \tag{2}$$

The situation is depicted in Figure 1

We assume that the surface tension is negligible so that the time dependent Bernoulli equation gives a dynamic boundary condition at the free surface,

$$\frac{\partial \psi}{\partial t} + \frac{1}{2}(\nabla\phi)^2|_{z=\eta} + g\eta = 0, \tag{3}$$

where without loss of generality we have taken the arbitrary function of time in the Bernoulli equation to be the atmospheric pressure divided by the density of the liquid. There is also a kinematic boundary condition on the surface and at the base of the liquid,

$$\frac{\partial \eta}{\partial t} = \frac{\partial \phi}{\partial z} \quad \text{on } z = \eta(\mathbf{x}, t) \tag{4}$$

$$\frac{\partial \phi}{\partial z} = 0 \quad \text{on } z = -h. \tag{5}$$

Boundary conditions (3,4,5), along with the Laplace equation (1) present a complete system to describe surface waves on the liquids surface. However they are non-linear and have trivial solution, $\eta = 0, \phi = 0$, describing the equilibrium state. We therefore linearize the system by assuming the surface steepness is small, so that we can neglect nonlinear terms in Equation (3) and assume that Equation (4) is evaluated at $z = 0$ rather than on the free surface [11]. The wave steepness is defined as,

$$\alpha = k\eta(\mathbf{k}). \tag{6}$$

The resulting problem can be solved using the standard Fourier transform in the (x, y) plane. For any function $f(x, y)$ we define the Fourier transform as follows

$$f(\mathbf{k}) = \frac{1}{2\pi}\int f(\mathbf{r})e^{-i(\mathbf{k}\cdot\mathbf{r})}\,\mathrm{d}\mathbf{r}$$
$$f(\mathbf{x}) = \frac{1}{2\pi}\int f(\mathbf{k})e^{i(\mathbf{k}\cdot\mathbf{x})}\,\mathrm{d}\mathbf{k} \tag{7}$$

where the function and its Fourier transform are distinguished by their argument for simplicity of notation.

The Laplace Equation (1) now takes the form

$$\frac{\partial^2 \phi(\mathbf{k}, z, t)}{\partial z^2} - k^2\phi(\mathbf{k}, z, t) = 0. \tag{8}$$

The solution to the system of equations (2,5,8) is given by,

$$\phi(\mathbf{k}, z, t) = \psi(\mathbf{k}, t)\frac{\cosh(kz + kh)}{\cosh kh} \tag{9}$$

where $k = |\mathbf{k}|$. Making the small surface steepness approximation in equations (4) and (3) taking the Fourier transform then substituting in equation (9) we have,

$$\frac{\partial \eta(\mathbf{k},t)}{\partial t} = k \tanh(kh)\psi(\mathbf{k},t) \tag{10}$$

$$\frac{\partial \psi(\mathbf{k},t)}{\partial t} = -g\eta(\mathbf{k},t) \tag{11}$$

assuming that $\eta(\mathbf{k},t) = \eta(\mathbf{k})e^{i\omega(k)t}$ and $\psi(\mathbf{k},t) = \psi(\mathbf{k})e^{i\omega(k)t}$ it follows that the dispersion relation for traveling surface gravity waves is;

$$\omega(\mathbf{k}) = \sqrt{gk \tanh kh} \tag{12}$$

As $h \to \infty$, $\tanh kh \to 1$ so in the deep water approximation $\omega(\mathbf{k}) = \sqrt{gk}$ and it is clear that waves with low wave number (long wave length) will 'feel' the depth of a finite tank more.

B. Hamiltonian formulation and four-wave resonance

It has been shown [12–15] that the dynamic and kinematic boundary conditions on the free surface describing the fluid flow are equivalent to a pair of Hamiltonian canonical equations in η and ψ which for a pair of canonically conjugate variables,

$$\frac{\partial \eta(\mathbf{x},t)}{\partial t} = \frac{\delta H}{\delta \psi(\mathbf{x},t)}, \quad \frac{\partial \psi(\mathbf{x},t)}{\partial t} = -\frac{\delta H}{\delta \eta(\mathbf{x},t)} \tag{13}$$

where δ represents a variational derivative, and the Hamiltonian $H = K + \Pi$ is the sum of kinetic (K) and potential (Π) energies divided by the fluid density. The kinetic and potential energy are given by,

$$K = \frac{1}{2}\int\int_{-h}^{\eta} (\nabla\psi)^2 \,\mathrm{d}z\,\mathrm{d}\mathbf{x} \tag{14}$$

$$\Pi = \frac{1}{2}g\int \eta^2 \,\mathrm{d}\mathbf{x} \tag{15}$$

where the integral with respect to $\mathbf{x}$ extends over the entire horizontal plane (assumed unbounded container of depth h).

The Fourier transform (Equation 7) is canonical so that the evolution equation (13) remains of the same Hamiltonian form (under the transformation). We introduce two new canonical variables derived from the Fourier transform of $\eta(\mathbf{x},t)$ and $\psi(\mathbf{x},t)$,

$$\eta(\mathbf{k}) = \mathcal{M}(\mathbf{k})\left(a(\mathbf{k}) + a^*(-\mathbf{k})\right), \quad \psi(\mathbf{k}) = -i\mathcal{N}(\mathbf{k})\left(a(\mathbf{k}) - a^*(-\mathbf{k})\right)' \tag{16}$$

where * represents the complex-conjugate and with

$$\mathcal{M} = \left(\frac{\omega(\mathbf{k})}{2}\right)^{\frac{1}{2}}, \quad \mathcal{N} = \left(\frac{1}{2\omega(\mathbf{k})}\right)^{\frac{1}{2}}. \tag{17}$$

Equation 13 then reduces to a single equation in k-space,

$$i\frac{\partial a(\mathbf{k})}{\partial t} = \frac{\delta H}{a^*(\mathbf{k})} \tag{18}$$

where H is now a functional of $a(\mathbf{k})$ and $a^*(\mathbf{k})$. Equation 18 and its complex-conjugate form the pair of canonical Hamilton equations.

Again assuming that the surface steepness is small (weekly nonlinear) the Hamiltonian, $H(a, a^*)$, can be formally expanded as an integral power series in a and a^*, for details see [11, 16],

$$H = \sum_{n=2}^{\infty} H^{(n)} \tag{19}$$

where $H^{(i)} < H^{(j)}$ if $i < j$ and $H^{(2)}$ corresponds to the linear approximation and is given by,

$$H^{(2)} = \int \omega(\mathbf{k}) a_k a_k^* \, \mathrm{d}k. \tag{20}$$

Higher order terms are of the general structure $H^{(n)} = \sum_{l=0}^{n} H_l^{(n)}$, where

$$H_l^{(n)} = \frac{1}{(l!m!)} \int V_{k_{l+1},\ldots,k_n}^{k_1,\ldots,k_l} (a_{k_1}^* \ldots a_{k_l}^* a_{k_{l+1}} \ldots a_{k_{l+m}}) \delta(k_1 + \ldots + k_l - k_{l+1} - \ldots - k_n) \, \mathrm{d}k_1 \ldots \mathrm{d}k_n, \tag{21}$$

$\delta(\cdot)$ is the Kronecker delta. The coefficients are given explicitly in [16]. This Hamilotnian can be reduced further by canonical transformations of a_k. However there arise non-integrable singularities in the coefficients of the canonical transformations near the manifolds,

$$\omega(\mathbf{k_1}) \pm \omega(\mathbf{k_3}) \pm \omega(\mathbf{k_3}) = 0, \quad \mathbf{k_1} \pm \mathbf{k_2} \pm \mathbf{k_3} = \mathbf{0}, \tag{22}$$

$$\omega(\mathbf{k_1}) + \omega(\mathbf{k_2}) - \omega(\mathbf{k_3}) - \omega(\mathbf{k_4}) = 0, \quad \mathbf{k_1} + \mathbf{k_2} - \mathbf{k_3} - \mathbf{k_4} = \mathbf{0}, \tag{23}$$

these are termed the resonance conditions. This problem is related to the problem of 'small devisors' in classical perturbation theory. However for surface gravity waves the dispersion relation, Equation 12, is concave and so the three wave resonance condition Equation (22) can not be satisfied. The non-resonat terms in the Hamiltonian that can be elminated by suitable canonical transformations, are in a sense, unimportant. So for surface gravity waves the lowest order (and therefore most important) non-linear wave interaction is the 4-wave interaction defined by Equaiton (23).

Assuming the nonlinearity is weak then time scale for the wave periods (linear dynamics) is much shorter than that of the nonlinear dynamics by which the wave modes exchange energy. Exploiting this time scale seperation one can take a suitable purturbation expansion of the conjugate variable (a_k) to focus on events arising due to nonlinearity. Further under the Random Phase and Amplitude (RPA) approximation [1], that the amplitude and phase are independent random variables and the phase of the conjugate variables is uniformly distributed, it is possible to derive a Kineitc Equation for the wave [2, 11]. This was first done by Hasselmann in 1962 [2] in terms of the wave-action spectrum n_k defined by the statistical average of the (squared) amplitude,

$$\frac{\partial n_k}{\partial t} = \int W_{\mathbf{k_1},\mathbf{k_2}}^{\mathbf{k_3},\mathbf{k}} \left(n_{k_1} n_{k_2} (n_{k_3} + n_k) - n_{k_3} n_k (n_{k_1} + n_{k_2}) \right) \delta(k_1 + k_2 - k_3 - k) \delta(\omega_1 + \omega_2 - \omega_3 - \omega) \, \mathrm{d}k_{1,2,3}, \tag{24}$$

which describes the rate of energy transfer due to 4-wave interactions. The interaction coefficient is given by,

$$W_{\mathbf{k_1},\mathbf{k_2}}^{\mathbf{k_3},\mathbf{k}} = \frac{9\pi g^2 D^2_{\mathbf{k_1},\mathbf{k_2},\mathbf{k_3},\mathbf{k}}}{4\rho^2 \omega_1 \omega_2 \omega_3 \omega}, \tag{25}$$

where D is given in the Appendix. Typically for $\omega_1 \leq \omega_2 \leq \omega_3 \leq \omega_4$ the net energy transfer is from ω_2 and ω_3 to ω_1 and ω_4.

Zakharov and Filonenko derived the following power law steady state solution to Equation (24)

$$n \sim k^{-4} \tag{26}$$

known as the Zakharov-Filonenko spectrum [3], describing the cascade of energy from low to high values of k. For analysis of the data we define the energy wave spectrum as,

$$E_f = \int e^{2\pi f t' i} \langle \eta(\mathbf{x}, t) \eta(\mathbf{x}, t + t') \rangle dt', \tag{27}$$

so that the Zakharov-Filonenko spectrum Equation (26) corresponds to $E_f \sim f^{-4}$. This has been observed in several numerical exeriments.

Other power law power spectra, $E_f \sim f^{-\nu}$, describing the energy cascade have been berived by alternative approaches. Most notably Philips derived $E_f \sim f^{-5}$ ($\nu = 5$), which can be derived from dimensional analysis assuming g is the only relavent dimensional physical quantity [5]. The argument is equivalent to the linear terms of the same order as the nonlinear terms in the wave equations in Fourier space and physically corresponds to sharp wave crests. Physically the Philips spectrum is associated with sharp wave crests leading to point discontinuties. Kuznetsov also derived a power-law power spectrum based on a linear dispersion relation for the wave crests with breaking on a D dimesional wavecrest giving $\nu = 3 + D$ [6]. Recently Nazarenko derived $E_f \sim f^{-6}$ ($\nu = 6$) for waves in a finite basin where k-space descreteness causes a sandpile type behaviour in the energy cascade [7] as briefly described below.

C. Discrete wave turbulence

We briefly describe the theory given in [4, 7] for the case of week turbulance in discrete k-space (fluid in finite box). For Equation (24) the limit of infinite region is taken before the limit of week nonlinearity, so that in a finite region for the conditions to be approximately satisfied the broadening of the 4-wave nonlinear resonance must be enough to cover the gap in k-space. If the forcing is small then the number of exact and quasi four-wave interactions may be significantly depleted [8, 17]. There still remain some exact and quasi resonaces before the nonlinear resonance broadening is of order of the k-space but they remain significantly depleted with respect to the continous case [4] and are insufficient to support a turbulance cascade.

In numerical simulations periodic boundary conditions are normally assumed so that for an L_x by L_y computational region the wave vector will be discretized by,

$$\mathbf{k} = \left(\frac{2\pi m}{L_x}, \frac{2\pi n}{L_y} \right), \quad m, n \in \mathbb{Z} \tag{28}$$

For the purpose of the physical experiment in a finite flume we assume that frictional effects and wave breaking at the edges [18] results in eigen modes that have nodes at the bounday, hence

$$\mathbf{k} = \left(\frac{\pi m}{L_x}, \frac{\pi n}{L_y} \right), \quad m, n \in \mathbb{Z}. \tag{29}$$

For wave-action spectrum of n at a frequency of ω the characteristic nonlinear time τ_{NL} is estimaed in [4] as,

$$\tau_{NL} \sim g^{10} \omega^{-19} n^{-2}, \tag{30}$$

corresponding to a resonance broadening in k-space given by

$$\kappa_{NL} = \frac{1}{\frac{\partial \omega}{\partial k} \tau_{NL}} \sim g^{-11} \omega^{20} n^2. \tag{31}$$

If the surface is intially at rest and forcing occurs at a narrow band of frequency then intially there will be no transfer of energy accross scales and the spectrum will grow at the driving mode approximately at the rate of energy input. This continues until the resonance broadening κ_{NL} is of the order of the k-spaceing at the driving frequency. At this point non linear energy transfer across scales will become activated and energy will be transfered to adjecent range of frequencies given by the resonance conditions. The condition on the surface steepness for the resonance broadening to be of order of the k-spacing derived in [4] is given by,

$$\alpha_c \sim 1/(kL)^{1/4}. \tag{32}$$

so that for $\alpha < \alpha_c$ energy transfer over scales is significantly reduced. If the forcing is week so that its characteristic time is significantly less than than τ_{NL} then the wave-action spectrum will never significantly exceed its critical value. The critical spectrum with κ_{NL} approximately the k-spacing will then occur accross the interial range resulting in $E_f \sim f^{-6}$.

III. EXPERIMENTAL SETUP

All experiments with surface gravity waves were conducted in a rectangular flume with dimension $12 \times 6 \times 1.5$ meters, or a trapezium flume where the length was reduced to 11.37m on the long side and 9.35m on the short side with a width of 6m. The flume was filled with water to a depth of 0.9m. Waves are generated by 8 vertical paddles of width 0.75m that span the short side of the flume, see Figure 2. Each panel can move independently of the others perpendicular to its face plane. Parameters of the desired wave field are specified to a motion control to set the driving amplitude, frequency distribution and wave vector direction.

For some of the experiments analysed in this work there was a single excited wave mode with direction perpendicular to the wave maker norm and frequency of 0.973Hz in the trapezium flume (signals no.s 352, 353 and 357). Experiments are also analysed for the rectangular flume with two driven wave modes, one perpendicular to the wave maker with frequency of 0.973Hz and the other at 1.14Hz at 9°, corresponding to wave vectors $(3.8099, 0)$ and $(5.1656, 0.8181)$ respectively (signal no.s 512, 513, 515). One further experiment is analysed for the rectangular flume with two driven wave modes, both perpendicular to the wave maker normal at 2.919Hz and 0.791Hz, (see Table I), for this experiment the depth was 0.8m.

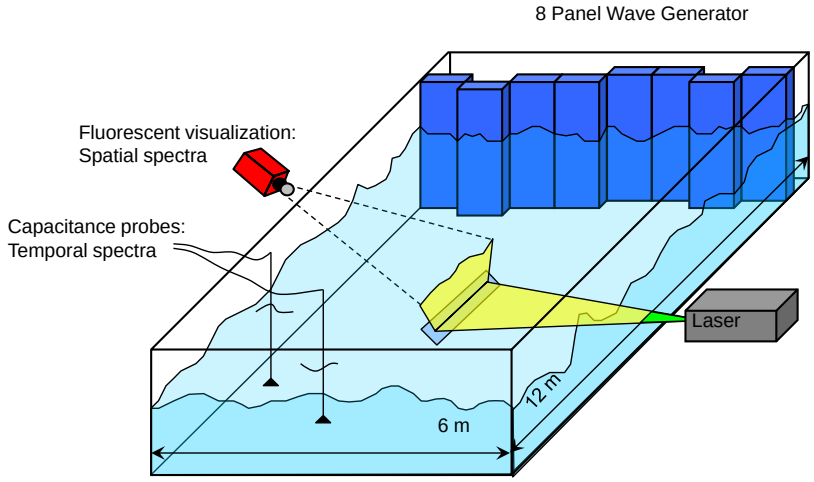

FIG. 2: Experimental setup, Total Environmental Simulator at "The Deep" Geography Department, University of Hull.

The surface elevation was measured simultaneously by two capacitance probes, positioned in the middle part of the flume, see Figure 2. Each probe consists of a wire covered by a thin isolating layer suspended vertically and partially submerged. Due to the difference in dielectric permeability of water and air the surface elevation can be derived from the capacitance between the probe and the wave tank. The capacitance was measured using sinusoidal AC with different frequencies for each probe to avoid cross talk. Signals from the probes were amplified (by lock-in amplifiers) and then digitized by a multi-functional board (NI6035, National Instruments) and stored as a waveform using LabView software. The sampling rate was 400Hz for each channel. The probes were calibrated before experiments in the same tank with a stationary water surface. Before each experiment the water was left to settle and reach an approximately stationary surface for a minimum of 15 minutes.

The dual surface elevation signals were processed using Matlab. The signal was decimated to a sampling frequency of 100Hz and the initial transient part of the signal was removed.

IV. RESULTS

Across the large majority of experiments there is an observed initial maximum of the wave amplitude recorded. This can be quantified in terms of the root mean squared (RMS) surface elevation,

$$A = \sqrt{\langle(\eta - \bar{\eta})^2\rangle}, \tag{33}$$

where η is the surface elevation and $\bar{\eta}$ is the mean surface elevation. The average $\langle\cdot\rangle$ is taken over 10 seconds intervals of the data. The RMS surface elevation is seen to grow initially as energy is fed into the closed system but at a time close to 100s (Table I) it rapidly decreases and subsequently we observe larger fluctuations with steady growth of the RMS elevation (Figure 3). The surface elevation gives an effective lower bound on the wave amplitude and is seen to initially grow in good accordance with predictions based on energy input from the wave maker, Figure 4. We investigate the extent to which the peak and subsequent decrease in RMS elevation can be attributed to the onset of nonlinear wave interactions.

The initial period of each experiment before the local maximum in RMS elevation can be well understood in terms of linear wave theory. For experiments with a single driving frequency we observe surfaces waves with the same frequency and increasing amplitude. For experiments with two driving frequencies we observe beating as described by the superposition of two waves with frequencies of the two driving frequencies. Consider two plain waves of frequency ω_1 and ω_2 corresponding to the two driving frequencies, we have

$$\sin(\omega_1 t) + \sin(\omega_2 t) = 2\cos\left(\frac{1}{2}(\omega_1 - \omega_2)t\right)\sin\left(\frac{1}{2}(\omega_1 + \omega_2)t\right), \tag{34}$$

which can be observed directly in Figure 4 and is confirmed across the experiments. This was confirmed by averaging the period from the minimums (absolute magnitude) for the enveloping wave and the higher frequency was estimated by averaging the period of peaks clearly within the enveloping wave in the data.

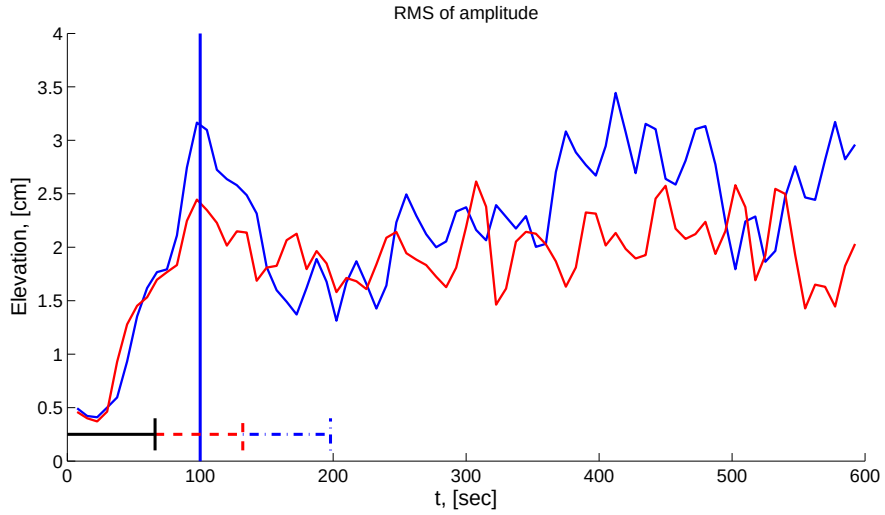

FIG. 3: RMS surface elevation (for signal 513) showing typical initial maximum marked by vertical line (blue). Channel one in blue and 2 in red. RMS taken over 10sec intervals. Intervals for spectra indicated below corresponding to colour and type used for time evolution spectral plots.

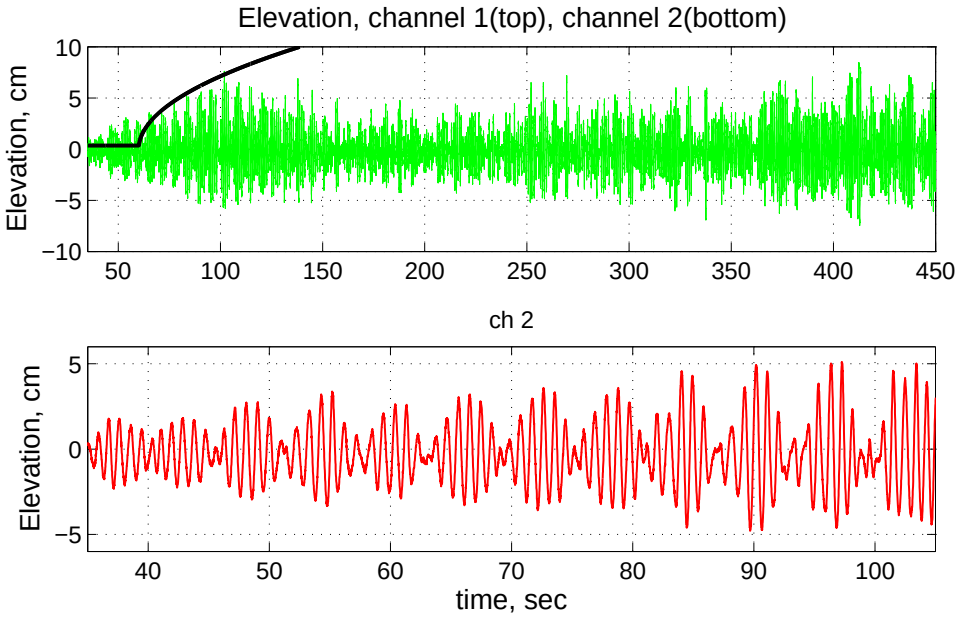

FIG. 4: Time Series of filtered data (for signal 513) as described in Section III. Top: 35-450s showing theoretical growth without dissipation as a solid line. Bottom: 35-105s of data, beating can be observed corresponding to linear theory.

The initial maximum of each signal was located by finding the maximum RMS elevation in the first 200s of the data. The results are summarized in Table I.

For a given frequency we can calculate an estimate of the critical amplitude given in Section II above which waves of that frequency (and lower) will 'feel' the finite size effects discussed in Section II. For each of the experiments (apart from signal 507 discussed later) the driving frequency is close to 1Hz, so that the wave-number (absolute value) that corresponds to the driving modes is

$$k_D \approx (2\pi)^2/g \approx 4m^{-1}. \tag{35}$$

The flume length is approximately 10m so that from Equation (32) we can estimate the critical amplitude at

TABLE I: Table of initial maximums (time and RMS elevation), flume dimension and driving modes. Starred signals are those for which spectral plots are given as example

Signal no.	Flume dimensions [m]	Driving freq.[Hz]		Left Ch. initial max		Right Ch. initial max	
		f_0	f_1	time ±10 [sec]	RMS ±0.2 [cm^2]	time ±10 [sec]	RMS ±0.2 [cm^2]
352*	$11.37/9.35 \times 6 \times 0.9$	0.973		125	5.83	95	10.67
353	$11.37/9.35 \times 6 \times 0.9$	0.973		125	2.24	105	2.87
357	$11.37/9.35 \times 6 \times 0.9$	0.973		95	1.10	95	1.46
512	$12 \times 6 \times 0.9$	0.973	1.140	105	3.81	165	3.39
513*	$12 \times 6 \times 0.9$	0.974	1.140	105	3.33	105	2.46
515	$12 \times 6 \times 0.9$	0.973	1.140	125	3.57	125	2.13
507	$12 \times 6 \times 0.9$	2.919	0.791	135	4.70	125	3.10

the driving frequency

$$A_c \sim \frac{1}{k(kL)^{1/4}} \sim 0.1m. \tag{36}$$

The surface elevation data gives an effective lower bound estimate for the amplitude of the driven modes at the initial maximum. For the experiments in the rectangular flume this is typically just over 5cm. Since Equation (36) is only an order of magnitude estimate a factor of two could easily be accounted for by an order one constant such as π. We observe for signal 352, in a trapezium flume, the waves reach a much greater amplitudes (approximately $\sqrt{2} \times 10$) during the inital maximum and subsequent nolinear effects are discussed below. The other signals in the trapezium flume were driven at a lower rate, they also show an intial maximum however there is a distinct difference in behaviour observed the spectral plots (Section IV A).

If we assume the amplitude reached by the system is of order 0.05m this gives an estimate for the frequency of waves that 'feel' the finite size of the flume as approximately 1.3Hz and below. This implies that nonlinear interactions may not be arrested across the range of frequencies observed in the flume, for instance a driving frequency close to 1Hz also excites a harmonic close to 2Hz which may then transfer energy to higher more dissipative frequencies more easily (as described in Section II). This is observed in many of the spectral in the next section.

A. Spectra

To find spectra we used the Welch algorithm with the Hanning window, for estimating the spectrum slope we used windows of length 1024 (10.24 s) with the averaging over about 500 spectra (Figures 5 7(a) 8). Horizontal lines show show the fit range over which the slope is estimated using linear least-square logarithmic fit, typically over less than one decade. However for signals 513-515 and 352 a 95% confidence interval from the least squares fit shows an error on the slope of less than ±0.2, this is small compared to errors estimated by changing the window size or varying the fitting range of around ±0.5.

For calculating the evolution of the spectra windows of length 2048 (20.48s) were used and the averaging was performed over a minimum of 5 spectra (Figures 6 7(b)). Spectra were calculated during the initial increase in amplitude (typically first 66s), then during the initial maximum and finally during the subsequent decrease in RMS elevation. Intervals given by the horizontal lines on Figure 3 show the time periods over which the spectra in Figure 6 were taken (corresponding colour and type).

The spectral slope for wave signal 513 in a rectangular flume with two driving frequencies is given by $\nu \sim 5.2 \pm 0.7$. This is in reasonable agreement (although slightly smaller magnitude) with the prediction $\nu = 6$ made in [7] for the critical spectrum where the nonlinear resonance broadening is of the same order of magnitude as the spacing in discrete k-space. This result was confirmed across signals 512, 513 and 507.

The spectra for signal 513, Figure 6, show initially a concentration of energy (E_f c.f Equation 27) at the two driving frequencies and close to their harmonics. During the maximum in the surface elevation ($66 - 132$s shown by red dashed line) there is an increase in energy predominately at these frequencies. During the subsequent decrease in RMS surface elevation ($132 - 198$s) it is clear that there is a decrease in the energy in the wave modes corresponding to the driving however there is a general increase across the rest of the spectrum. The spectrum then more closely resembles the critical spectra predicted theoretically. This suggests that nonlinear

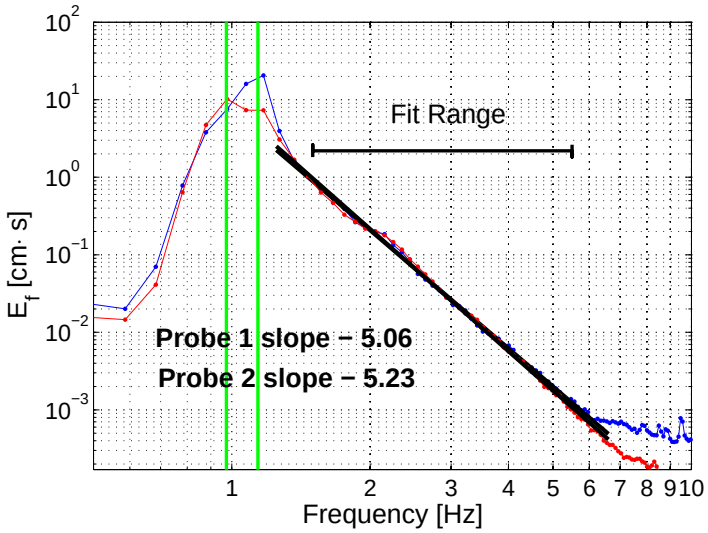

FIG. 5: Spectral slope estimate for signal 513 showing critical exponent close to −6. Green vertical lines show the driving frequencies

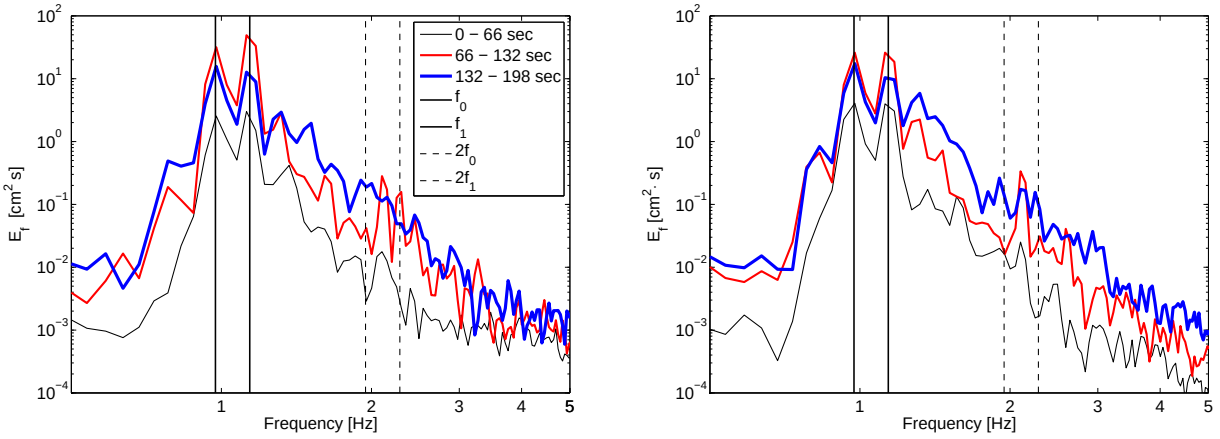

(a)Left channel (b)Right channel

FIG. 6: Spectra before during and after initial peak confirmed for signals 512 − 515 (results for 513 shown) (two driving frequencies close to 1Hz in rectangular flume). Vertical lines show the driving frequencies (broken for harmonics)

wave interactions are then more active allowing transfer of energy through the scales to the more dissipative higher frequencies. This same behaviour has also been confirmed across signals 512, 513 and 507.

We observe similar behaviour as in the rectangular flume, with two driving frequencies, in the trapezium flume (Signal 352) with a single strong driving frequency. Initially energy is concentrated at the driving frequency and corresponding harmonics. During the maximum of the RMS surface elevation E_f at the driving frequency and the first harmonic also reach a maximum. After the initial maximum E_f decreases at the driving frequency and its harmonic and there is a general increase across the rest of the spectrum. We therefore associate the fall in RMS surface elevation after the initial maximum with a 'filling out' of the spectrum before reaching an approximately power-law power spectrum over the range from the driving frequency to the dissipation scale. It appears from this analysis (Figures 6 and 7(b)) that the process by which the system approaches a power lower power spectrum occurs quicker for higher frequencies, this supports the theory that higher frequencies feel k-space discreteness less and the non-linear time scale for higher frequencies is much shorter, c.f. Equation (30).

Figure 7(b) shows a spectral estimate after the initial maximum showing the approach to a power law power spectrum, with exponent $\nu \sim 4.3$, between the driving frequency and the high frequency cut off of the inertial

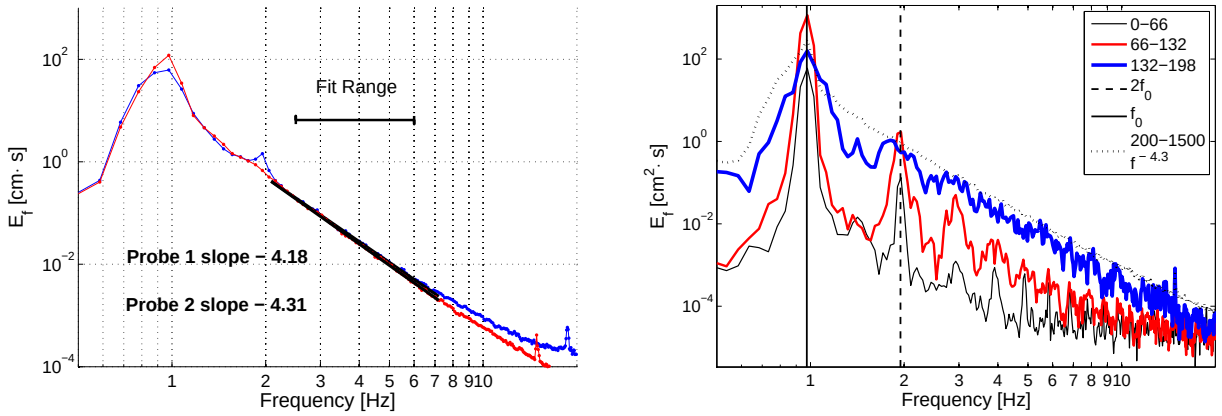

(a) Spectrum slope

(b) Time evolution

FIG. 7: Left: Estimate of spectrum slope for signal 352 in a trapezium flume with high driving rate Right: Spectra before during and after initial peak for signal 352 in trapezium flume with high driving rate. Behaviour is specific to case of high driving rate for experiments in a trapezium flume.

range. The exponent is in good agreement with theoretical predictions such as the ZF spectrum and Kuznetsov theory (Section II). However the RMS elevation reaches very high values implying very high nonlinearity which invalidates assumptions that form the basis of the ZF spectrum [7]. Kuznetsov theory [6] which considers strongly nonlinear waves with sharp wave crest 1D ridges is therefore more applicable and also derives a $\nu = 4$ power law power spectrum [10].

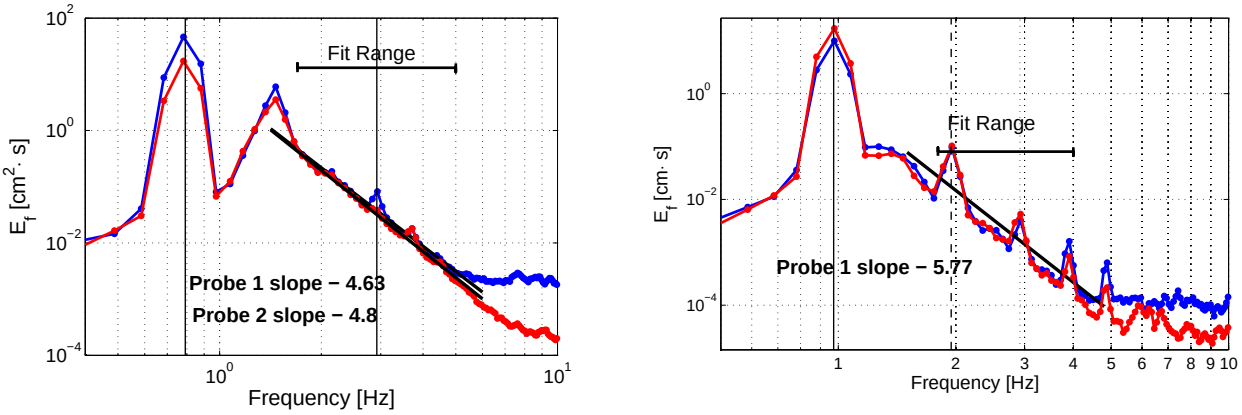

(a) Signal 507 slope

(b) Signal 353 slope

FIG. 8: Left: Spectra for signal 507 in a rectangular flume, and with low driving rate, taken across entire signal whilst being driven. Driven at two well separated frequencies shown by green vertical lines. Cascade appears at higher frequencies and an accumulation close to the lower driving frequency. Right: Spectra for signal 353 in trapezium flume with a single driving frequency with a relatively low rate, spectrum is dominated by the driving frequency and harmonics, cascade type power law power spectrum is never reached.

For the experiment corresponding to wave signal 507 waves were excited at two driving frequencies, one relatively high 2.919Hz and one relatively low 0.791Hz, in a rectangular flume (Table I). The power spectra for this experiment, Figure 8(a), shows that at frequencies higher than the first harmonic of the lowest driving frequency (1.582Hz) the spectrum approximately reaches a power law power spectrum corresponding to the theoretically predicted energy cascade. However at lower frequencies there is an accumulation of energy at the lowest driving frequency suggesting that resonance broadening in this region never reaches a level sufficient to fully activate a large number nonlinear wave interactions. This supports the argument that lower frequencies 'feel' the finite size of the flume more strongly.

For experiments in the trapezium flume with low driving rate (signals 353 and 357) we observe that the spectrum is dominated by the driving frequency and subsequent harmonics, Figure 8(b). A fully developed power law power spectrum is never reached. This suggests that nonlinear wave interactions are never sufficiently active to cause an efficient cascade across the inertial range.

B. 4-wave resonant interactions

Assuming that energy is quickly dissipated from modes that do not have nodes at the boundary walls gives a discrete $\mathbf{k}-$space lattice for the flume defined by

$$\mathbf{k}_{m,n} = \left(\frac{m\pi}{L_x}, \frac{n\pi}{L_y}\right), \tag{37}$$

where L_x is the length of the flume and L_y is the width of the flume. For the rectangular flume (signals 507, 512, 513, and 515) the lattice is shown by black dots on Figure 9(a). The resulting discreteness in frequency space can be calculated from the dispersion relation Equation 12, close to the driving frequency of 1Hz this is given by

$$2\pi|\omega(\mathbf{k}_{m,n}) - \omega(\mathbf{k}_{m+1,n})| \approx 0.033 \text{ Hz}. \tag{38}$$

This is smaller than the frequency resolution on the spectra plots (Figures 6) of 0.0488Hz Since the surface gravity wave dispersion relation is concave the spacing of Eigenmode frequencies also decrease as the frequency increase. We therefore can not distinguish different Eigen-modes directly from the Spectra.

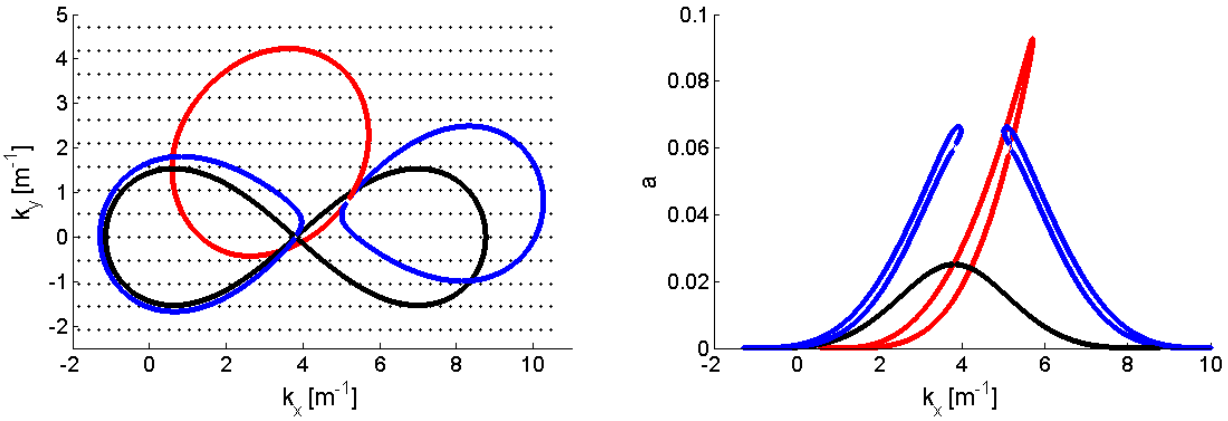

(a) Resonant manifold

(b) Interaction coefficient

FIG. 9: Left: $\mathbf{k}_4$ on the resonance manifold defined by $\mathbf{k}_1 + \mathbf{k}_2 = \mathbf{k}_3 + \mathbf{k}_4$ and $\omega_1 + \omega_2 = \omega_3 + \omega_4$. Black dots show Eigen-modes of the rectangular flume. Black; Philips figure-8 curve when $\mathbf{k}_1 = \mathbf{k}_2$ corresponds to the low frequency driving mode [19]. Blue; $\mathbf{k}_1$ corresponds to the low frequency driving mode, $\mathbf{k}_2$ corresponds to the high frequency driving mode. Red; $\mathbf{k}_1$ corresponds to the low frequency driving mode, $\mathbf{k}_3$ corresponds to the high frequency driving mode. Right: The value of the interaction coefficient ($a = W$), Eq. (25), on the resonant manifold

The resonance manifold defined by Equations (23) is shown in Figure 9(a) ($\mathbf{k}_4$ is plotted which along with two driving modes fully specifies the resonant manifold) for various combinations of the two driving modes as well as the $\mathbf{k}-$space lattice. The mode corresponding to the 0.973Hz driving frequency is given by $\mathbf{k}_{d1} = (3.810, 0)$ and the mode corresponding to the 1.14Hz driving frequency at 9^o to the wave maker normal $\mathbf{k}_{d2} = (5.166, 0.818)$. The Phillips figure-8 curve [19] can be observed as a solution to the resonance conditions,

$$2\mathbf{k}_{d1} = \mathbf{k}_3 + \mathbf{k}_4, \tag{39}$$

$$2\omega_{d1} = \omega_3 + \omega_4. \tag{40}$$

The resonant manifolds specify an interval in frequency space over which 4-wave interactions of the form $2\omega_{d1} = \omega_3 + \omega_4$ or $\omega_{d1} + \omega_{d2} = \omega_3 + \omega_4$ occur, this is given by $[0.6, 1.6]$Hz.

The rate of energy transfer inferred by the interaction coefficient W (Equation 25) is largest for interactions of the form $\mathbf{k}_{d1} + \mathbf{k}_2 = \mathbf{k}_{d2} + \mathbf{k}_4$ at values of $\mathbf{k}_4$ corresponding to frequencies close to the 1.25Hz. The interaction coefficient is smaller for interactions on the Philips figure-8 curve relative to interactions of the form $\mathbf{k}_{d1} + \mathbf{k}_{d2} = \mathbf{k}_3 + \mathbf{k}_4$ (shown in blue). The rate of energy transfer is also affected by the wave action spectrum as shown by Equation (24). However this suggests that the interactions that occur at the fastest rate are those involving energy transfered away from both driving modes simultaneously.

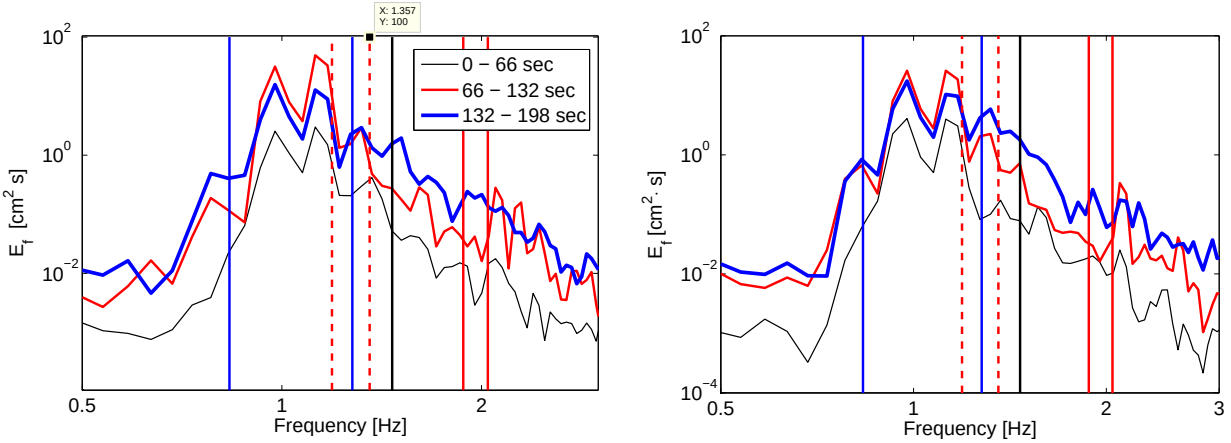

(a)Left channel (b)Right channel

FIG. 10: Time evolution of spectra for signal 513. Vertical lines show the closest quasi-resonances of the driving modes with Eigen-modes of the flume. Colours correspond with Figure 9. Broken vertical lines show a second closest quasi resonance.

We find the closest quasi-resonances with Eigen modes assuming that the wave maker excites the closest Eigenmodes to the driving modes ($\tilde{\mathbf{k}}_{d1}$ and $\tilde{\mathbf{k}}_{d2}$ respectively) for the three cases plotted in Figure 9. These are found by solving

$$\hat{\mathbf{k}}_4 = \arg\min_{\mathbf{k}_4} |\omega(\mathbf{k}_1) + \omega(\mathbf{k}_2) - \omega(\mathbf{k}_3) - \omega(\mathbf{k}_4)|, \tag{41}$$

where two of the modes are $\tilde{\mathbf{k}}_{d1}$ or $\tilde{\mathbf{k}}_{d2}$ and the third is specified uniquely by the resonace condition on the k-space lattice. colinear solutions are not considered since they make no contribution to the transfer of energy [20]. The corresponding quasi-resonances are displayed as vertical lines on Figures 10. The minimum resonance width in order to allow each of these interactions is summarized below,

$$\begin{aligned} |2\omega(\tilde{\mathbf{k}}_{d1}) - \omega(2\tilde{\mathbf{k}}_{d1} - \hat{\mathbf{k}}_4) - \omega(\hat{\mathbf{k}}_4)| &= 0.0003 \quad \text{black vertical line} \\ |\omega(\tilde{\mathbf{k}}_{d1}) + \omega(\tilde{\mathbf{k}}_{d2}) - \omega(\tilde{\mathbf{k}}_{d1} + \tilde{\mathbf{k}}_{d2} - \hat{\mathbf{k}}_4) - \omega(\hat{\mathbf{k}}_4)| &= 0.0052 \quad \text{blue vertical line} \\ |\omega(\tilde{\mathbf{k}}_{d1}) - \omega(\tilde{\mathbf{k}}_{d2}) + \omega(\tilde{\mathbf{k}}_{d2} - \tilde{\mathbf{k}}_{d1} + \hat{\mathbf{k}}_4) - \omega(\hat{\mathbf{k}}_4)| &= 0.0051 \quad \text{red vertical line.} \end{aligned} \tag{42}$$

These are much closer than are required for wave turbulence theory to apply (c.f Section II) since $(\partial w/\partial k)2\pi/L \approx 0.2$. For interactions of the three forms considered there are typical around ten (unique up to obvious symtery conditions) quasi fourwave interactions with $\delta_w < 0.1$, where $\delta_w = |w_1 + w_2 - w_3 - w_4|$.

V. DISCUSSION

In this work we have studied energy transfer by nonlinear wave interactions from experiments exciting one or two wave modes in a finite flume (both rectangular and trapezium shaped). Our main observation derived from the experimental results is that an initial maximum in RMS surface elevation (wave amplitude) corresponds to an accumulation of energy at the driving frequency and a subsequent decrease in RMS surface elevation occurs as energy is transferred across scales in k-space. This supports recent theoretical and numerical studies on wave turbulence in finite regions [4, 7] for which there is a threshold wave intensity bellow which nonlinear resonance broadening is insufficient to allow an energy cascade. Since the initial maximum was observed across a large proportion of experiments it is at this stage unclear how much can be attributed to the discrete k-space

and to what extent it is due to the relatively long characteristic time scale for nonlinear interactions (Equation (30)). Further, a single experiment in the trapezium flume with low driving intensity (signal 357) shows 'bursty' behaviour in which the RMS surface elevation continues to rise and fall similarly to the initial maximum. This seems to support theoretically predicted 'sandpile' behaviour [7] where discreteness in k-space (due to finite region) leads to an accumulation of energy at the driving scale causing widening of the nonlinear resonance which then triggers a cascade of energy away from the forcing scale and the cycle repeats, however further experiments will need to be conducted to confirm this phenomena. When the driving rate was low and there was only a single low driving frequency the spectrum was dominated by linear effects such as excitation of harmonics of the driving mode.

Results of such experiments could have major impact on harbour management. One of the major features seen in our results is that experiments with a single driving mode or where the two driving modes are well spaced (signal 507) see greater accumulation of energy near the lowest driving frequency and do not form as clear a critical power-law spectrum compared to those with two driving modes at similar frequencies (512,513 and 515). This can feasibly be explained in terms of non-communicating clusters of interacting wave modes when considering only exact resonances with Eigenmodes [9], if other interactions are assumed to be less significant. If such results can be confirmed it may be possible to excite a few (suitably chosen) modes in harbours that would support an energy cascade away from waves with a dangerously long wavelength. The flume shape may also play a role in the development of nonlinear wave interactions since in the trapezium shaped flume the Eigenmodes were disturbed, however to gain a fuller understanding of this would require more experiments and analysis.

We have found that quasi resonances of the driving modes with Eigen modes of the flume appear to be the first to become excited close to the initial maximum in RMS surface elevation. However due to the lack of resolution in frequency space further studies would have to fully confirm these results. Finding such quasi resonant and exact resonant quartets could be useful in identifying suitable modes to excite in Harbours to most efficiently transfer energy away from excited modes with long wavelength. More efficient ways of calculating exact resonant quartets in discrete k-space have been developed [17] that can make this task computationally much quicker than exhaustive methods used here. It is also possible that under certain circumstances (in larger flumes or Harbours) that although three wave interactions are ruled out for gravity waves because the dispersion relation is concave in k quasi three wave interactions may occur [21].

The value of the interaction coefficient we present is based on the analysis by Hasselmann [2], however we have argue that fundamental assumptions made in this derivation are not met. It would therefore be desirable to have an estimate of such coefficients under week nonlinearity and k-space discreteness.

Our analysis has relied heavily on the Fourier transform of the experimental data, however it is clear that the process is not time stationary across the windows that many of the transform have been taken. However preliminary results from a wavelet decomposition method (over time and scale) seem to support the results stated. A more detailed analysis in this direction could put the arguments made on a more rigorous footing.

To further support our findings numerical simulations could be performed along side continued laboratory experiments. Theoretical results could be more directly assessed in terms of numerical simulations which may show qualitatively similar behaviour as the experiments. For experiments studied in this work modes are excited by moving paddles horizontally at a velocity independent of the deth in the liquid. This cause eddy currents which directly violate the basic assumption in wave theory of irrotational flow, complicating a study of finite size effects. A more suitable driving could be used that matches the theoretical velocity profile for surface gravity waves. For example taking the derivate with respect to x of the Fourier transform of Equation (9). Therefore future experiments with more suitable driving and that could record information to help identify wave modes as well as frequencies could be of great benefit in this area.

Acknowledgements

I thank Petr Denissenko for volounteering the mini-project and for supervising the project. I would also like to thank Sergey Nazarenko for co-supervision and Colm Connaughton for many useful discussions. All experiments were completed at the total environment simulator at "The Deep", University of Hull Geography Department. Data was supplied by Sergyei Lukaschuk and Petr Denissenko. Finally I thank those involved in the Complexity DTC for its' support and tuition and the EPSRC for funding.

APPENDIX

We give D from the interaction coefficient α in Equation (25) as derived by Hasselmann [2],

$$D_{\mathbf{k_1},\mathbf{k_2},\mathbf{k_3},\mathbf{k}} = D^{+,+,-}_{\mathbf{k_3},\mathbf{k},-\mathbf{k_2}} = D^{+,+,-}_{\mathbf{k_3},\mathbf{k},-\mathbf{k_1}} = D^{+,+,-}_{\mathbf{k_1},\mathbf{k_3},-\mathbf{k}} = D^{+,+,-}_{\mathbf{k_1},\mathbf{k_2},-\mathbf{k_3}},$$

$$D^{s_1,s_2,s_3}_{\mathbf{k_1},\mathbf{k_2},-\mathbf{k_3}} = \frac{1}{3}\left(\hat{D}^{s_1,s_2,s_3}_{\mathbf{k_1},\mathbf{k_2},\mathbf{k_3}} + \hat{D}^{s_2,s_3,s_1}_{\mathbf{k_2},\mathbf{k_3},\mathbf{k_1}} + \hat{D}^{s_3,s_1,s_2}_{\mathbf{k_3},\mathbf{k_1},\mathbf{k_2}}\right)$$

$$\begin{aligned}\hat{D}^{s_1,s_2,s_3}_{\mathbf{k_1},\mathbf{k_2},\mathbf{k_3}} =& \frac{iD^{s_2,s_3}_{\mathbf{k_2},\mathbf{k_3}}}{\omega^2_{\mathbf{k_2}+\mathbf{k_3}} - (\omega_2+\omega_3)^2}\left(2(\omega_1+\omega_2+\omega_3)\left(\frac{w_1^2\omega^2_{\mathbf{k_2}+\mathbf{k_3}}}{g^2} - \mathbf{k_1}\cdot(\mathbf{k_2}+\mathbf{k_3})\right) - \frac{\omega_1(\mathbf{k_2}+\mathbf{k_3})^2}{\cosh(|\mathbf{k_2}+\mathbf{k_3}|h)}\right)\\
&- iD^{s_2,s_3}_{\mathbf{k_2},\mathbf{k_3}}\frac{\omega_1}{g^2}(\omega_1^2+\omega^2_{\mathbf{k_2}+\mathbf{k_3}}) + E^{s_2,s_3}_{\mathbf{k_2},\mathbf{k_3}}\left(\frac{\omega_1^3(\omega_2+\omega_3)}{g} - g\mathbf{k_1}\cdot(\mathbf{k_2}+\mathbf{k_3})\right)\\
&+ \frac{\omega_1}{2g^2}(\mathbf{k_2}\cdot\mathbf{k_3})\left((\omega_1+\omega_2+\omega_3)(\omega_2^2+\omega_3^2)+\omega_2\omega_3(\omega_2+\omega_3)\right)\\
&- \frac{\omega_1\omega_2^2k_3^2}{2g^2}(\omega_1+\omega_2+2\omega_3) - \frac{\omega_1\omega_3^2k_2^2}{2g^2}(\omega_1+2\omega_2+\omega_3),\end{aligned}$$

where

$$\begin{aligned}D^{s_1,s_2}_{\mathbf{k_1},\mathbf{k_2}} &= i(\omega_1+\omega_2)(k_1k_2\tanh k_1h\tanh k_2h - (\mathbf{k_1}\cdot\mathbf{k_2})) - \frac{i}{2}\left(\frac{\omega_1k_2^2}{\cosh k_2h} + \frac{\omega_2k_1^2}{\cosh k_1h}\right)\\
E^{s_1,s_2}_{\mathbf{k_1},\mathbf{k_2}} &= \frac{1}{2g}\left((\mathbf{k_1}\cdot\mathbf{k_2}) - g^{-2}\omega_1\omega_2(\omega_1^2+\omega_2^2+\omega_1\omega_2)\right)\end{aligned}$$

---

[1] Y. Choi, Y. V. Lvov, S. Nazarenko, Wave Turbulence, in "Recent developments in fluid dynamics" **5**, 225 (2004)
[2] K. Hasselmann, On the non-linear energy transfer in a gravity wave spectrum, J. Fluid Mech, **15**, 273-281 (1963)
[3] V. E. Zakharov, N. N. Filonenko. J. Appl. Mech. Tech. Phys. **4**, 506-515 (1967)
[4] Y. V. Lvov, S. Nazarenko, B. Pokorni Discreteness and its effect on the water-wave turbulence, Physica D **218**, 24 (2006)
[5] O. M. Phillips, The equilibrium range in the spectrum of wind generated waves. J. Fluid Mech. **4**, 426-434 (1958)
[6] E. A. Kuznetsov, Turbulence spectra generated by singularities, JETP Letters, **80**, 83-89 (2004)
[7] S. Nazarenko, Sandpile behavior in discrete water-wave turbulence, J. Stat. Mech. L02002 (2006) doi:10.1088/1742-5468/2006/02/L02002 (arXiv:nlin.CD/0510054).
[8] M. Tanakaa, N. Yokoyamab, Effects of discretization of the spectrum in water-wave turbulence, FDR, **34**, 199 216, (2004)
[9] E. Kartashova, S. Nazarenko, O. Rudenko Resonant interactions of nonlinear water waves in a finite basin, Phys. Rev. E, **78**, 016304 (2008)
[10] P. Denissenko, S. Lukaschuk1, S. Nazarenko, Gravity surface wave turbulence in a laboratory flume Phys. Rev. Lett. 99, 014501 (2007)
[11] V. E. Zakharov, Surface wave theory, Notes
A. Stewart, Turbulence in Surface Gravity Waves, Assessed project for the Taught Course Centre course 'Wave Turbulence'
[12] L. J. F. Broer. On the hamiltonian theory of surface waves. Applied Scientific Res., **30**, 430446 (1974)
[13] J. W. Miles. On hamilton's principle for surface waves. J. Fluid Mech., **83**, 153158 (1977)
[14] V. E. Zakharov, The Hamiltonian formalism for waves in nonlinear media having dispersion, Radiophys. Quantum Electronics **17**, 326-343 (1975)
[15] V. E. Zakharov, Stability of periodic waves of finite amplitude on the surface of deep fluid. J. Appl. Mech. Tech. Phys. (English transl.) **2**, 190-194 (1968).
[16] V. P. Krasitskii, Reduced equations in the Hamiltonian theory of weakly nonlinear surface waves, J. Fluid Mech, **272**, 1-20 (1994)
[17] E. Kartashova, Exact and quasi-resonances in discrete water-wave turbulence, Phys. Rev. Lett, **98** (21): 214502 (2007)
[18] C. C. Mei, L. F. Liu, The damping of surface gravity waves in a bounded liquid, J. Fluid Mech, **59**, 2, 239-256 (1973)

[19] 0. M. Phillips, On the dynamics of unsteady gravity waves of finite amplitude, J. Fluid Mech. **9** (1960) 193.
[20] A. I. Dyachenko, V. E. Zakharov, Is free-surface hydrodynamics an integrable system? Phy. Lett A, **190**, 144-148 (1994)
[21] A. M. Balk, Surface gravity wave turbulence: three wave interaction? Phy. Lett A, **314**, 6871 (2003)